Solar-Terrestrial Physics. 2022. Vol. 8. Iss. 3. P. 51–57. DOI: 10.12737/stp-83202208. © 2022 Shalimov S.L., Solovieva M.S. Published by INFRA-M Academic Publishing House

UDC 551.515.2, 551.510.535, 537.877
DOI: 10.12737/stp-83202208

Received March 30, 2022
Accepted June 06, 2022

IONOSPHERIC RESPONSE TO THE PASSAGE OF TYPHOONS OBSERVED BY SUBIONOSPHERIC VLF RADIO SIGNALS

S.L. Shalimov
Schmidt Institute of Physics of the Earth RAS, Moscow, Russia, pmsk7@mail.ru
Space Research Institute RAS, Moscow, Russia

M.S. Solovieva
Schmidt Institute of Physics of the Earth RAS, Moscow, Russia, rozhnoi@ifz.ru

Abstract. The response of the lower ionosphere to the passage of several dozen typhoons has been studied using a regional network of VLF stations in the Russian Far East. The experimental data presented in all cases clearly demonstrates wavelike disturbances of the subionospheric VLF signal amplitude and phase during the active stage of typhoons crossing radio paths. With the exception of magnetoactive and seismoactive days, this means that the disturbances generated by a typhoon, when propagating into the upper ionosphere, pass through the lower ionosphere, causing corresponding disturbances in the amplitude and phase of the VLF signal. Spectral analysis shows that the range of the wave disturbances detected corresponds to the periods of atmospheric internal gravity waves (IGW). A mechanism of the action of IGWs on the lower ionosphere is proposed which allows us to interpret the VLF signal phase variations observed. According to this mechanism, the action of IGW on the lower ionosphere is caused by polarization fields arising during the wave motion of plasma in the lower part of the F layer. These fields projected along geomagnetic field lines into the lower ionosphere cause the upper wall of the Earth—ionosphere waveguide to rise or fall.

Keywords: remote sensing by subionospheric VLF signals, atmospheric internal gravity waves, typhoons, ionosphere.

INTRODUCTION

Tropical cyclones and typhoons are considered among a number of meteorological factors that have a noticeable effect on plasma of the upper atmosphere [Danilov et al., 1987]. As estimated [Forbes et al., 2000], the electron density N_e perturbation in the F2-layer maximum, generated by meteorological factors, may run to 35 % of the background level under quite geomagnetic conditions. Calculated azimuths and horizontal velocities of some traveling ionospheric disturbances (TIDs) of meteorological origin have shown that the probable generation zones of TIDs detected are located in the troposphere and coincide with low atmospheric pressure areas in the regions of cyclone formation [Bertin et al., 1975]. Statistical studies on 24 strong typhoons in 1987–1992 indicate that medium-scale TIDs are often detected which are thought to be caused by turbulence of the lower atmosphere and generation of atmospheric acoustic-gravity waves when a strong typhoon makes landfall or is located near the coast [Xiao et al., 2007; Sharkov, 2012]. Observations of hydroxyl airglow have revealed [Suzuki et al., 2013] that at mesospheric heights disturbances associated with the passage of a typhoon form a pattern of concentric circles. This suggests that atmospheric internal gravity waves (IGW), which feature a similar spatial dispersion, can propagate directly from the typhoon region into the ionosphere. It has also been found [Zakharov, Kunitsyn, 2012] that typhoon-induced IGWs often go before a typhoon and propagate mainly along its path. It should, however, be kept in mind that IGW can propagate from the troposphere to the ionosphere only if the wind structure is favorable for such propagation, namely, the wind should be directed toward the propagating atmospheric wave. While atmospheric waves are considered to be the main link connecting the typhoon zone with the ionosphere, the mechanisms of the effect of such waves on the ionosphere receive almost no attention. As a result, some researchers find a possible response in the lower (by means of rockets) [Vanina-Dart et al., 2008] and upper (via GPS) [Vanina-Dart, 2011; Yasyukevich et al., 2013] ionosphere, whereas others (via GPS) [Afraimovich et al., 2008] do not. It is therefore obvious that the specific features of the ionospheric response to the passage of typhoons should continue to be studied using capabilities of global and regional networks, as well as various monitoring tools. It is new research with additional tools that can identify the mechanisms of the impact of typhoons on the ionosphere.

In this paper, we make use of a regional network of stations of remote sensing by subionospheric VLF radio signals to study the ionospheric response to the passage of typhoons. Specifics of the experiment consists in applying a convenient method of remote sensing of the effects on the ionosphere — recording amplitude-phase characteristics of signals from low-frequency (LF) and VLF radio stations. Frequencies of these signals (3–30 kHz) are such that they are capable of propagating thousands of kilometers from a transmitter to a receiver with weak attenuation (~2 dB per 1000 km) in the natural Earth—ionosphere

waveguide (reflection from the ionosphere occurs at altitudes of ~60 km during the day and ~85 km at night). The amplitude and phase of the signals are sensitive indicators of the state of the ionosphere. If atmospheric waves are generated by a typhoon, they, when propagating into the upper ionosphere, pass through the lower ionosphere, and the corresponding disturbances of the VLF signal amplitude and phase will be an indicator of this process. Similar ideas formed the basis for the search for the ionospheric response to the effects of earthquakes and tsunamis on the ionosphere [Rozhnoi et al., 2012, 2014a; Shalimov et al., 2019].

Note that the research into the ionospheric response to the passage of typhoons via remote sensing by subionospheric VLF signals is just at the initial stage. In the only work on this topic [Rozhnoi et al., 2014b] we know, it has been shown that this method is very effective for detecting the effects of atmospheric waves on the ionosphere.

INSTRUMENTS AND MEASUREMENT DATA

The receiving stations of subionospheric VLF radio signals of the regional network in the Russian Far East are located in Petropavlovsk-Kamchatsky, Yuzhno-Sakhalinsk, and Yuzhno-Kurilsk. The stations are equipped with UltraMSK receivers [http://ultramsk.com], which simultaneously measure the amplitude and phase of MSK (Minimum Shift Keying) modulated signals in the frequency band 10–50 kHz from several transmitters. The MSK signals have fixed frequencies in the range 50–100 Hz relative to the fundamental frequency. A receiver can record signals with a sampling step from 50 ms to 60 s. For the analysis we have used data with a time interval of 20 s.

We have analyzed VLF signal variations for 35 typhoons over the period 2014–2021, which crossed zones of path sensitivity (five Fresnel zones) during weak magnetic and seismic activity, i.e. in the absence of events with Dst<–50 nT and magnitude M>5.5. Other sources of such signal disturbances may be volcanic eruptions or tsunamis. Yet no such events occurred during the time period considered. The analysis was made for the amplitude and phase of the signal from an NWC transmitter (19.8 kHz), located on the west coast of Australia. We have used data obtained at the receiving stations in Petropavlovsk-Kamchatsky (PTK), Yuzhno-Sakhalinsk (YSH), and Yuzhno-Kurilsk (YUK) (Figures 1, 4). The data in Petropavlovsk-Kamchatsky was obtained by the Kamchatka Branch of the Federal Research Center "Geophysical Service of the Russian Academy of Sciences" [http://www.gsras.ru/new/infres]. Abnormal variations in the signal amplitude and phase have been found for eighteen cases.

Results of the analysis are presented in Table. Data on typhoons was taken from the website of the Japan Meteorological Agency (JMA) [https://www.jma.go.jp/jma/indexe.htmll]. Table shows that seventeen events did not have the expected effect. The reasons for the absence of signal anomalies in these cases call for further investigation, but it should be noted (and this circumstance has been mentioned in Introduction) that the most likely reason is the wind structure unfavorable for IGW propagation into the ionosphere (when the wind direction coincides with the direction of wave propagation, critical layers for waves are formed).

As the ionosphere is quite stable and insensitive to weak effects during the daytime, we took a nighttime interval for the analysis. Since VLF signals have diurnal and seasonal variations, we used a differential signal, defined as the difference between observed and monthly average signals. Then this signal was averaged over the nighttime interval. Below are examples of the analysis of VLF signal variations for two typhoons: Faxai and Nepartak.

Typhoon Faxai (TC 1915) reached a typhoon category on September 6, 2019; on September 8, the typhoon achieved its maximum strength and was categorized as a category 4 typhoon on the Saffir-Simpson Hurricane Wind Scale (SSHWS). The typhoon weakened on September 9 when it reached the coast of Japan [http://agora.ex.nii.ac.jp/digital-typhoon/summary/wnp/s / 201915.html.en]. All day on September 8, the typhoon was in the sensitivity zones of three NWC signal paths (Figure 1). Signal amplitude variations for the three paths are shown in Figure 2. For some time on September 7, Faxai moved inside the sensitivity zone of the NWC–PTK path; and for a shorter time, inside the NWC–YUK path. Along these paths, the signal amplitude decreased on September 7 and 8. Along the NWC–YSH path, a sharp drop in amplitude was recorded on September 8 (see Figure 2).

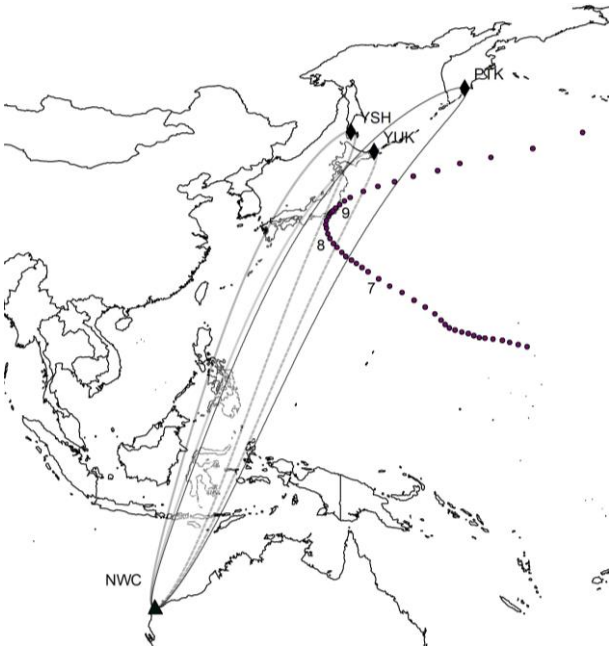

Figure 1. Mutual arrangement of an NWC transmitter (triangle) and receiving stations (rhombuses) in Petropavlovsk-Kamchatsky (PTK), Yuzhno-Sakhalinsk (YSH), and Yuzhno-Kurilsk (YUK). Ellipses indicate sensitivity zones of signal propagation paths. Dots show the path of typhoon Faxai (TC 1915) in September 2019. Numbers are dates of motion of the typhoon

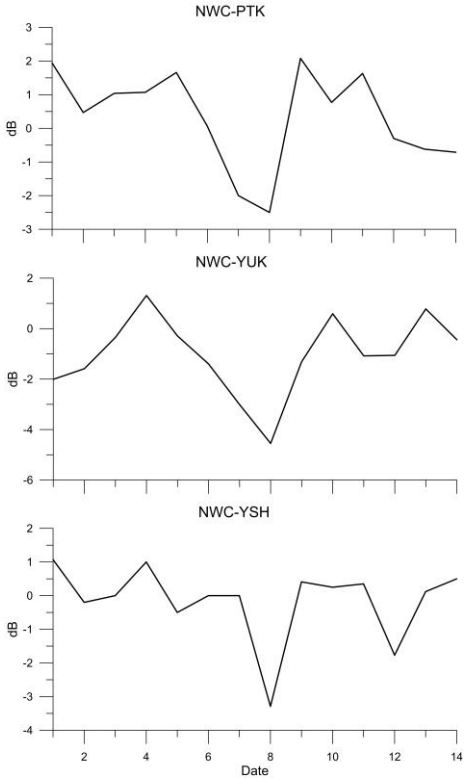

Figure 2. Variations in the NWC signal amplitude for the three paths shown in Figure 1. Difference signal values averaged over the nighttime interval are presented. Along the X-axis are dates in September 2019.

For that day, we carried out a wavelet analysis of the amplitude and phase of the nighttime signal filtered in the frequency range 0.3–15 mHz (Figure 3). The filter was selected in such a way as to examine the periods from 1 to 55 min. In this range there are atmospheric acoustic and internal gravity waves separated by the Brunt-Väisälä frequency. The maximum spectral density was found to have a period ~16–20 min; therefore, further we analyzed the 8–55 min disturbance periods, which represent the range of IGW disturbances.

Typhoon Nepartak (TC 1601) reached Category 4 strength on July 4, 2016. It was rated as Category 5 (SSHWS) on July 5, 2016. The next day, the typhoon reached its peak intensity. Nepartak began to weaken slightly on July 7, remaining a typhoon [http://agora.ex.nii.ac.jp/digital-typhoon/summary/wnp/s/201601.html.en].

The typhoon's path is shown in Figure 4. Variations in the VLF signal amplitude for the NWC–PTK and NWC–YSH paths are depicted in Figure 5. An amplitude depression was observed on July 5 along the NWC–PTK path and on July 5–7 along NWC–YSH. The wavelet analysis of the amplitude and phase for July 5 and 7 is illustrated in Figures 6 and 7 respectively.

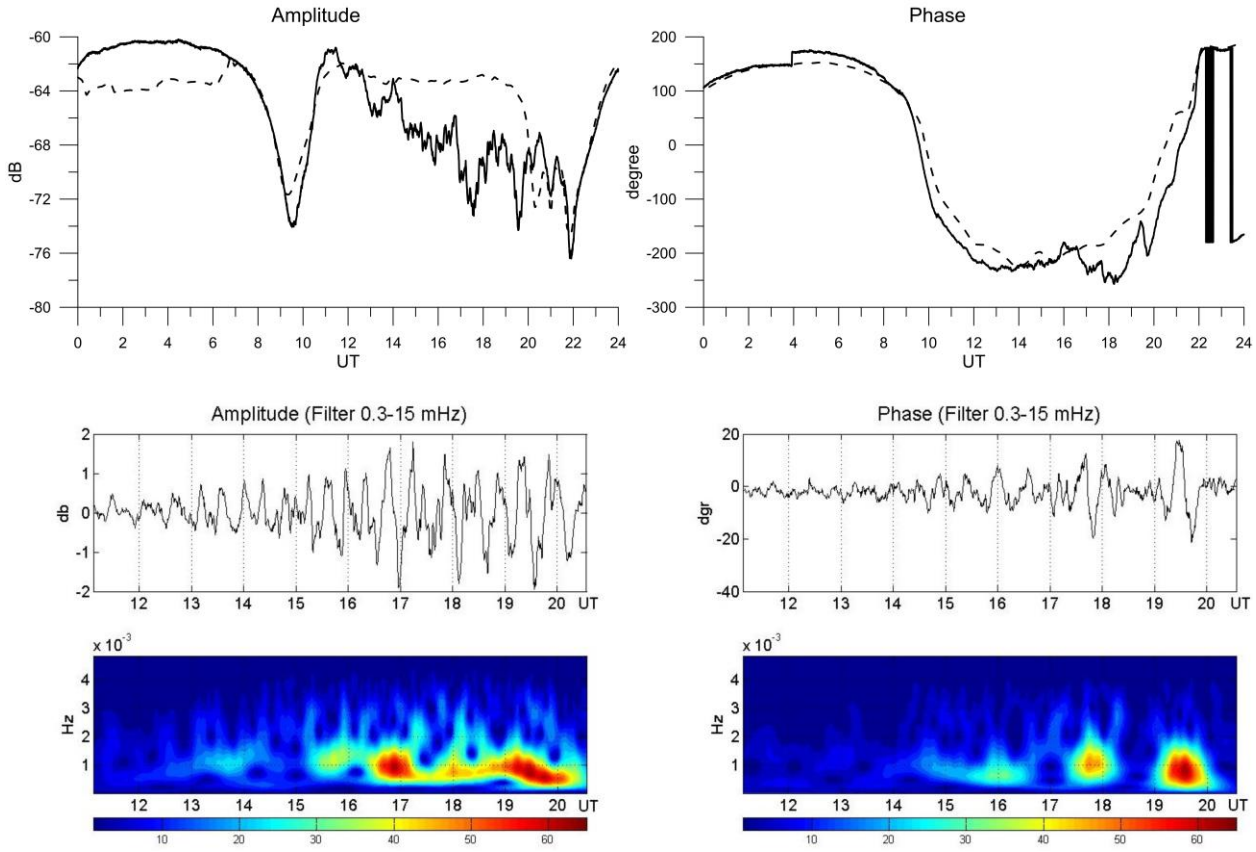

Figure 3. Amplitude and phase: top panels — of an NWC signal recorded in Yuzhno—Sakhalinsk on September 8, 2019 (solid line) and a monthly average signal (dashed line); middle panels — of a nighttime filtered signal along the same path. Bottom panels show wavelet spectra of the filtered signal

Presence/absence of disturbances in VLF signal during the passage of typhoons

Name	International Number	Category SSHWS	Duration	Maximum wind speed at 1 min interval, km/hr	Presence/absence of disturbances
Neoguri	TC 1408	5	July 2–11, 2014	260	–
Rammasun	TC 1409	5	July 9–20, 2014	260	+
Halong	TC 1411	5	July 27 – August 11, 2014	260	+
Phanfone	TC 1418	4	September 28 – October 6, 2014	250	–
Vongfong	TC 1419	5	October 2–14, 2014	215	+
Hagupit	TC 1422	5	November 30 – December 12, 2014	285	+
Maysak	TC 1504	5	March 27 – April 7, 2015	230	–
Noul	TC 1506	5	May 2–12, 2015	260	–
Soudelor	TC 1513	5	July 29 – August 11, 2015	285	–
Goni	TC 1515	4	August 13–25, 2015	220	+
Koppu	TC 1524	4	October 12–21, 2015	240	+
Melor	TC 1527	4	December 10–17, 2015	230	+
Nepartak	TC 1601	5	July 2–10, 2016	285	+
Meranti	TC 1614	5	September 8–17, 2016	315	–
Chaba	TC 1618	5	September 24 – October 7, 2016	280	–
Haima	TC 1622	5	October 14–21, 2016	270	+
Nock-ten	TC 1626	5	December 20–28, 2016	280	+
Noru	TC 1705	4	July 19 – August 8, 2017	250	–
Lan	TC 1721	4	October 15–23, 2017	250	+
Jebi	TC 1821	5	August 26 – September 4, 2018	285	–
Cimaron	TC 1820	4	August 16–24 , 2018	215	+
Mangkhut	TC 1822	5	September 6–17 , 2018	285	–
Trami	TC 1824	5	September 20 – October 1 , 2018	260	+
Kong-rey	TC 1825	5	September 28 – October 7 , 2018	280	–
Yutu	TC 1826	5	October 21 – November 3 , 2018	280	–
Lekima	TC 1909	4	August 2–14 , 2019	250	–
Faxai	TC 1915	4	September 2–9 , 2019	215	+
Hagibis	TC 1919	5	October 4–22 , 2019	295	–
Kammuri	TC 1928	4	November 24 – December 6 , 2019	220	+
Maysak	TC 2009	4	August 27 – September 7, 2020	230	–
Goni	TC 2019	5	October 26 – November 6, 2020	315	–
Vamco	TC 2022	4	November 8–15 , 2020	215	+
Surigae	TC 2102	5	April 12 – May 2 , 2021	305	+
Chanthu	TC 2114	5	September 5– 20, 2021	285	+
Mindulle	TC 2126	5	September 22 – October 2 , 2021	265	–

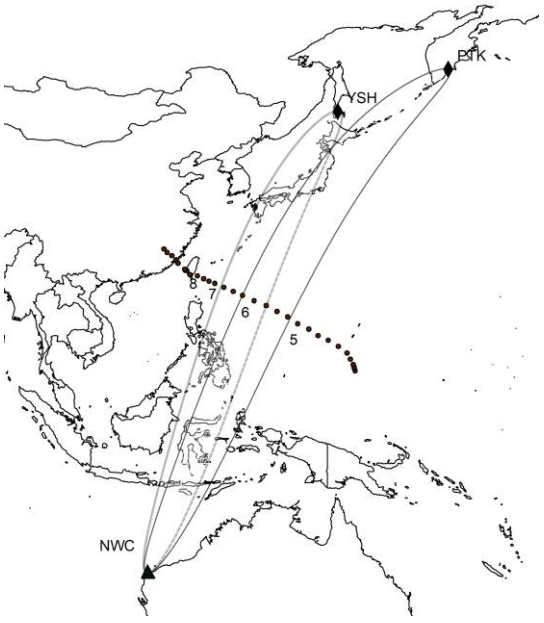

Figure 4. Path of typhoon Nepartak in July 2016. Designations are the same as in Figure 1

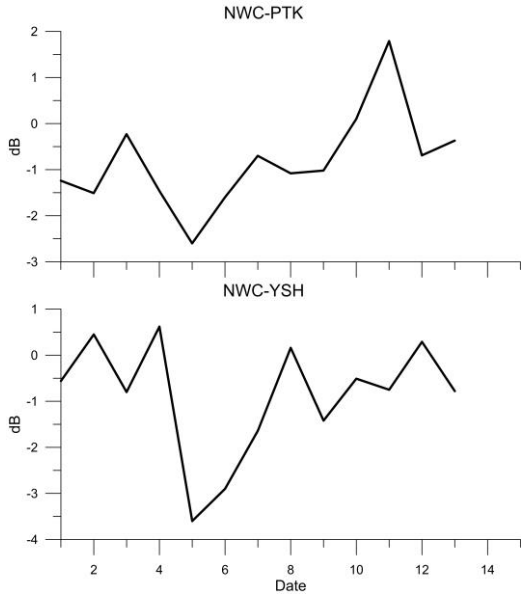

Figure 5. Variations in the NWC signal amplitude for two paths shown in Figure 4. Designations are the same as in Figure 2

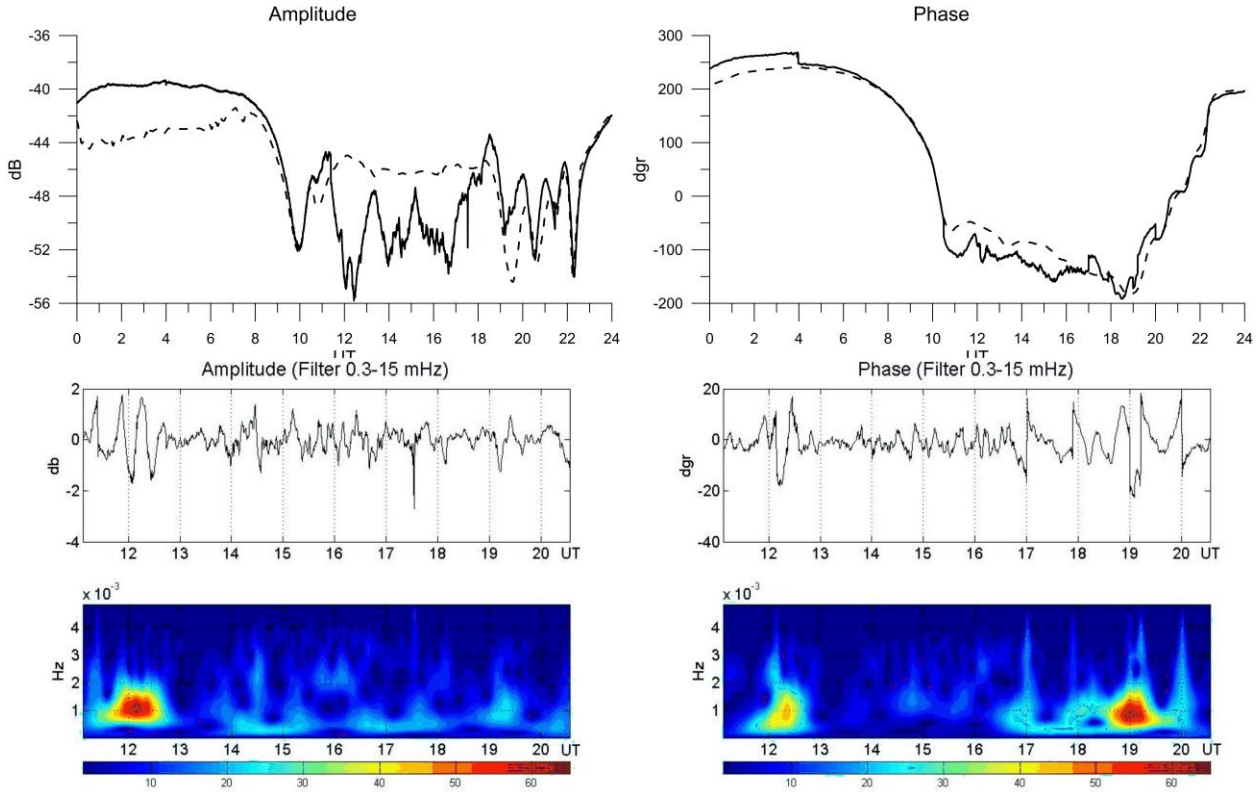

Figure 6. The same as in Figure 3, but for July 5, 2016 along the NWC–PTK path

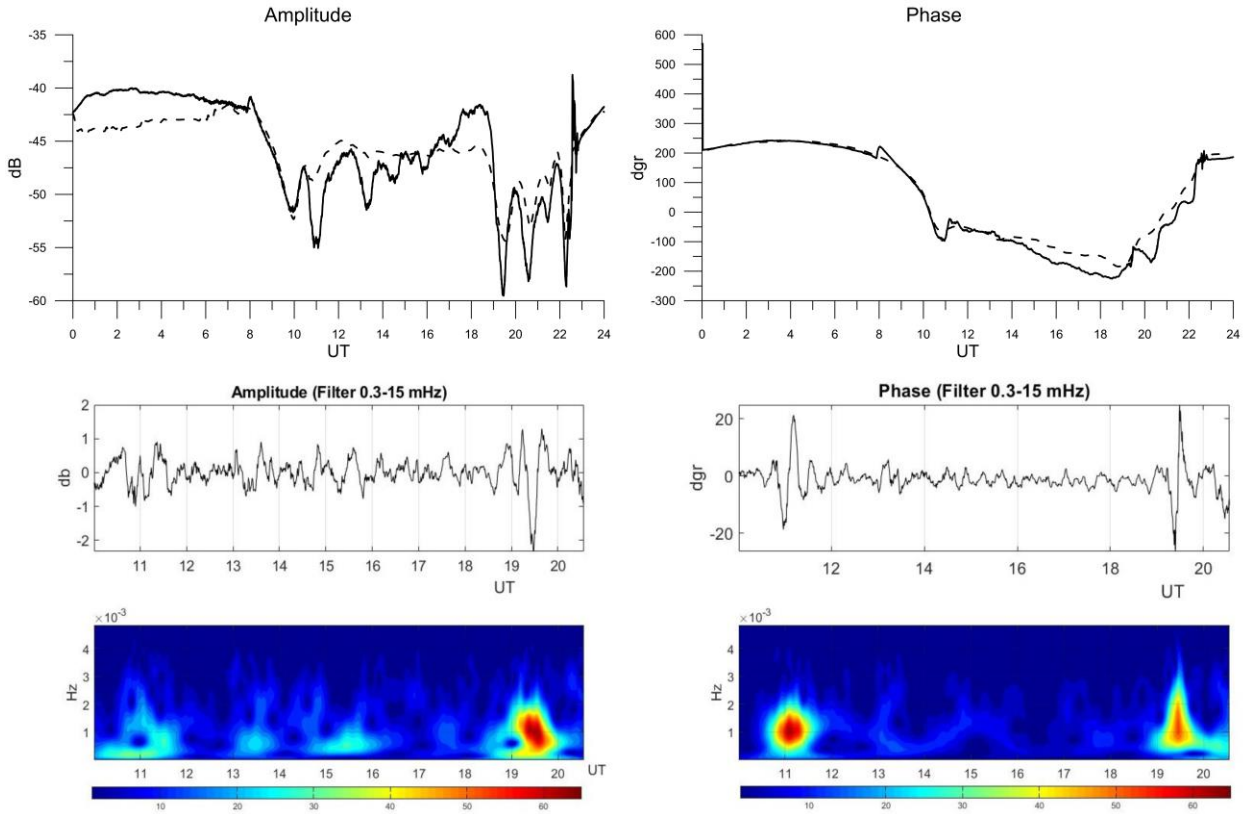

Figure 7. The same as in Figure 3, but for July 7, 2016 along the NWC–YSH path

DISCUSSION AND CONCLUSION

The experimental data presented clearly demonstrates wave disturbances of the VLF signal amplitude and phase during the active phase of typhoons (for other typhoons, measurements for which are omitted, this conclusion is valid too). The wavelet analysis shows the presence of waves in the period range 8–55 min (Figures 3, 6, 7). This range corresponds to atmospheric IGWs. With GPS satellites, Chou et al. [2017a, b] have made direct observations of variations in the total electron content (TEC) in the above mentioned period range for typhoon Nepartak.

The idea that typhoons generate IGWs is certainly not new. Moreover, the idea itself has been repeatedly confirmed by direct detection of wave disturbances in the upper ionosphere, which were associated with the passage of typhoons (see, e.g., [Chou et al., 2017a, b]). In particular, it has been found [Zakharov, Kunitsyn, 2012] that the IGWs induced by a typhoon are ahead of the typhoon and propagate mainly along its path.

Nonetheless, due attention has not been paid to the mechanism of the impact of typhoon-generated IGW on ionospheric plasma, leading to the observable effects (in particular in the D layer of the ionosphere). It is necessary to take into account here that unlike acoustic waves, IGWs at ionospheric heights are vertically transverse waves whose group velocity is perpendicular to the phase one and hence the wave energy propagates at a right angle to the direction of propagation of the wavefront. If a typhoon crosses a VLF path, as shown in Figures 1 and 4, the atmospheric wave generated by it propagates in the near-equatorial ionosphere almost across the geomagnetic field lines. In this case, wind disturbances $\delta\mathbf{U}$ are directed across the geomagnetic field so that currents $\delta\mathbf{j}=\sigma_P(\delta\mathbf{U}\times\mathbf{B}_0)$ arise in the wave propagating to the lower part of the F layer. If the currents are not divergence-free, polarization electric fields $\delta\mathbf{E}$ appear which cause the plasma to move in the direction $\delta\mathbf{E}\times\mathbf{B}_0$. A scheme of these processes for propagating IGW is given in Figure 8. The motion occurs along the wave front, and the magnetic field is directed out of the plane of the drawing.

Since the motion of the medium in the wave is counter, the currents are not divergence-free even in a homogeneous plasma. This gives rise to alternating layers of different signs with electric fields corresponding to the wavelength. The electric field component perpendicular to the magnetic field in the dipole magnetic field is projected into the lower ionosphere. In this case, the vertical plasma drift component generates disturbances in the form of rising and falling plasma sheets, which correspond to the horizontal wavelength. As a result, the rise and fall in the plasma sheets in the D-region lead to a decrease and increase in the phase, i.e. to phase variations with the period of the dominant wave. It is essential that the plasma velocity in the disturbances does not exceed the velocity of neutral motions since at $\delta\mathbf{E}=-(\delta\mathbf{U}\times\mathbf{B}_0)$ the plasma velocity $\delta\mathbf{v}=(\delta\mathbf{E}\times\mathbf{B}_0)/B_0^2=\delta\mathbf{U}$.

Note that the scheme in Figure 8 is idealized as there are conditions when polarization electric fields may be shorted. Firstly, magnetic field lines in the equatorial F-region, bending, penetrate the E-region outside the equator, whose daytime conductivity is high (in this paper, we analyze the nightside ionosphere). Secondly, if the wave vector $\mathbf{k}$ is not strictly perpendicular to the field line, currents along the magnetic field prevent the formation of charge layers. This determines the certain direction of the impact of the typhoon's IGW on ionospheric plasma.

Lastly, there may be conditions when a wave moves along the geomagnetic field (or there is a field-aligned velocity component). Such a situation may arise due to the specific spatial dispersion of IGW, which manifests itself in the formation of concentric disturbance zones. At the same time, the motion of neutrals along the magnetic field due to collisions involves plasma in the accompanying motion. With sufficiently slow motions characteristic of IGW, the rise and fall in the plasma column are accompanied (in particular in the F layer of the ionosphere) by an increase and decrease in the electron density. This is the situation that must have taken place at the final stage of the development of typhoon Nepartak (July 07, 2016), when TEC wave disturbances in the form of concentric arcs were recorded by GPS to the north of the typhoon location [Chou et al., 2017b].

Note that in addition to the mechanism proposed in this paper there is another mechanism of the effect of IGW on the D-region due to IGW dissipation (see [Rozhnoi et al., 2012]). The passage of the supposed acoustic weak shock waves and IGW through the D-region cannot generate the observable wave disturbances of VLF signal phase and amplitude because of the specific character of plasma at these heights (electrons are magnetized, whereas ions are not), where the effect of wind shear is necessary to redistribute the plasma vertically (in the E-region, this leads to the formation of sporadic layers [Gershman, 1974]). That is why, although acoustic and weak shock waves can cause additional ionization [Kozlov, 2021], there is no wind shear in this case. Wind shear occurs for IGW, yet this mechanism is ineffective at heights of the D-region (see, e.g.,

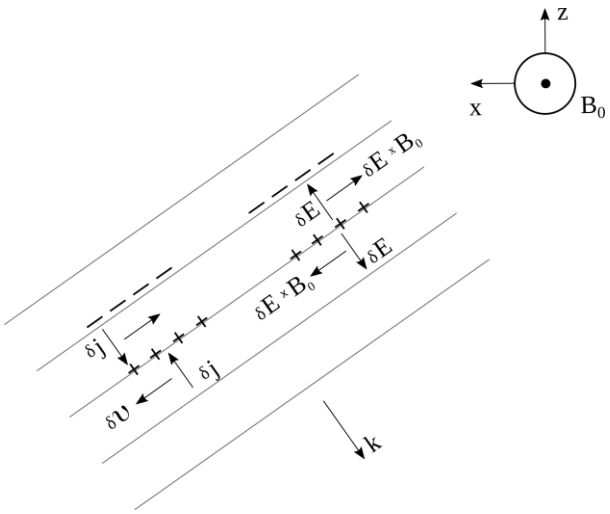

Figure 8. Scheme of electric field generation by wind disturbances in IGW

[Haldoupis, Shalimov, 2021]), and there is practically no vertical redistribution of plasma (necessary to explain the VLF signal phase and amplitude variations).

Thus, studying the ionospheric response to the passage of typhoons by means of a regional network of stations of remote sensing by subionospheric VLF radio signals allows us to establish quite clearly that the typhoon-generated IGW reaching the ionosphere under favorable conditions can cause VLF signal phase and amplitude variations. The proposed mechanism of the IGW effect on the lower ionosphere is due to the polarization fields that arise during the wave motion of plasma in the lower part of the F layer, which, projected along the magnetic field lines into the lower ionosphere, cause the upper wall of the Earth—ionosphere waveguide to go up or down. In turn, such motions are responsible for the variations in the VLF signal phase.

The work was financially supported by the Russian Science Foundation (Grant No. 22-27-00182). The data in Petropavlovsk-Kamchatsky was collected by the Kamchatka Branch of the Federal Research Center "Geophysical Service of the Russian Academy of Sciences" with financial support from the Ministry of Science and Higher Education of the Russian Federation (Government Assignment No. 075-00576-21).

REFERENCES

Afraimovich E.L., Voyeikov S.V., Ishin A.B., Perevalova N.P., Ruzhin Yu.Ya. Total electron content variations during the powerful typhoon of August 5–11, 2006, near the southeastern coast of China. *Geomagnetism and Aeronomy*. 2008, vol. 48, no. 5, pp. 674–679. DOI: 10.1134/S0016793208050113.

Bertin F., Testud J., Kersley L. Medium scale gravity waves in the ionospheric F-region and their possible origin in weather disturbances. *Planet. Space Sci*. 1975, vol. 23, pp. 493–507.

Chou M.Y., Lin C.H., Yue J., Tsai H.F., Yang Yi Sun, Jann Yenq Liu, Chia Hung Chen. Concentric traveling ionosphere disturbances triggered by Super Typhoon Meranti (2016). *Geophys. Res. Lett*. 2017a, vol. 44, iss. 3, pp. 1219–1226. DOI: 10.1002/2016GL072205.

Chou M.Y., Lin C.H., Yue J., Chang L.C., Ho-Fang Tsai, Chia-Hung Chen. Medium-scale traveling ionospheric disturbances triggered by Super Typhoon Nepartak (2016). *Geophys. Res. Lett*. 2017b, vol. 44, iss. 15, pp. 7569–7577. DOI: 10.1002/2017GL073961.

Danilov A.D., Kazimirovsky E.S., Vergasova G.V., Khachikyan G.Ya. *Meteorologicheskie effekty v ionosfere* [Meteorological Effects in the Ionosphere]. Leningrad, Gidrometeoizdat Publ., 1987, 267 p. (In Russian).

Forbes J.M., Palo S.E., Zhang X. Variability of the ionosphere. *J. Atmos. Solar-Terr. Phys*. 2000, vol. 62, pp. 685–693. DOI: 10.1016/S1364-6826(00)00029-8.

Gershman B.N. *Dinamika ionosfernoi plazmy* [Ionospheric Plasma Dinamics]. Moscow, Nauka Publ., 1974, 262 p. (In Russian).

Haldoupis C., Shalimov S. On the altitude dependence and role of zonal and meridional wind shears in the generation of E region metal ion layers. *J. Atmos. Solar-Terr. Phys*. 2021, vol. 214, 105537. DOI: 10.1016/j.jastp.2021.105537.

Kozlov S.I. *Aeronomiya iskusstvenno vozmushchennykh atmosfery i ionosfery* [Aeronomy of artificially disturbed atmosphere and ionosphere of the Earth]. Moscow, Torus Press Publ., 2021, 268 p. (In Russian).

Rozhnoi A., Shalimov S., Solovieva M., Levin B., Hayakawa M., Walker S. Tsunami-induced phase and amplitude perturbations of subionospheric VLF signals. *J. Geophys. Res.* 2012, vol. 117, iss. A9, A09313. DOI: 10.1029/2012JA017761.

Rozhnoi A., Solovieva M., Levin B., Hayakawa M., Fedun V. Meteorological effects in the lower ionosphere as based on VLF/LF signal observations. *Natural Hazards and Earth System Sciences*. 2014a, vol. 14, iss. 10, pp. 2671–2679. DOI: 10.5194/nhess-14-2671-2014.

Rozhnoi A., Shalimov S., Solovieva M., Levin B., Shevchenko G., Hayakawa M., Hobara Y., Walker S.N., Fedun V. Detection of tsunami-driven phase and amplitude perturbations of subionospheric VLF signals following the 2010 Chile earthquake. *J. Geophys. Res.: Space Phys.* 2014b, vol. 119, iss. 6, pp. 5012–5019. DOI: 10.1002/2014JA019766.

Shalimov S.L., Rozhnoi A.A., Solov'eva M.S., Ol'shanskaya E.V. Impact of Earthquakes and Tsunamis on the Ionosphere. *Izvestiya. Physics of the Solid Earth*. 2019, vol. 55, iss. 1, pp. 168–181.

Sharkov E.A. *Global Tropical Cyclogenesis*. Springer Praxis Books, 2012, 604 p.

Suzuki S., Vadas S. L., Shiokawa K., Otsuka Y., Kawamura S., Murayama Y. Typoon-induced concentric airglow structures in the mesopause region. *Geophys. Res. Lett.* 2013, vol. 40, iss. 22, pp. 5983–5987. DOI: 10.1002/ 2013GL058087.

Vanina-Dart L.B., Pokrovskaya I.V., Sharkov E.A. Equatorial lower ionosphere reaction upon strong tropical disturbances. *Geomagnetism and Aeronomy*. 2008, vol. 48, no. 2, pp. 255–260. (In Russian).

Vanina-Dart L.B., Romanov A.A., Sharkov E.A. Influence of tropical cyclone upon the upper ionosphere according to tomographic sounding over Sakhalin in 2007. *Geomagnetism and Aeronomy*. 2011, vol. 51, no. 6, pp. 790–798. (In Russian).

Xiao Z., Xiao S.G., Hao Y.Q., Zhang D.H. Morphological features of ionospheric response to typhoon. *J. Geophys. Res*. 2007, vol. 112, iss. A4, A04304. DOI: 10.1029/2006JA011671.

Yasukevich Yu.V., Edemsky I.K., Perevalova N.P., Polyakova A.S. Ionospheric response upon helio- and geophysical disturbing factors according to GPS. Irkutsk: ISU Publ., 2013, 160 p. (In Russian).

Zakharov V.I., Kunitsyn V.E. Regional features of atmospheric manifestations of tropical cyclones according to ground based GPS network data. *Geomagnetism and Aeronomy*. 2012, vol. 52, no. 4, pp. 533–545. DOI: 10.1134/S0016793212040160.

URL: http://ultramsk.com (accessed May 20, 2022).

URL: http://www.gsras.ru/new/infres (accessed May 20, 2022).

URL: https://www.jma.go.jp/jma/indexe.html (accessed May 20, 2022).

URL: http://agora.ex.nii.ac.jp/digital-typhoon (accessed May 20, 2022).

Original Russian version: Shalimov S.L., Solovieva M.S., published in Solnechno-zemnaya fizika. 2022. Vol. 8. Iss. 3. P. 54–61. DOI: 10.12737/szf-83202208.

How to cite this article

Shalimov S.L., Solovieva M.S. Ionospheric response to the passage of typhoons observed by subionospheric VLF radio signals. *Solar-Terrestrial Physics*. 2022. Vol. 8. Iss. 3. P. 51–57. DOI: 10.12737/stp-83202208.